Engineering Structures 254 (2022) 113807

Contents lists available at ScienceDirect

Engineering Structures

journal homepage: www.elsevier.com/locate/engstruct

Design of a novel seismic retrofitting system for RC structures based on asymmetric friction connections and CLT panels

Angelo Aloisio [a,c,*], Francesco Boggian [b,c], Roberto Tomasi [c,*]

[a] Department of Civil, Construction-Architectural and Environmental Engineering, Università degli Studi dell'Aquila, L'Aquila, Italy
[b] Department of Civil, Environmental and Mechanical Engineering, Università degli Studi di Trento, Trento, Italy
[c] Faculty of Science and Technology, Norwegian University of Life Sciences, Ås, Norway

ARTICLE INFO

Keywords:
Friction-based device
Seismic protection
Structural design
Reinforced-concrete structures
Timber engineering

ABSTRACT

Friction-based dampers are a valid solution for non-invasive seismic retrofitting interventions of existing structures, particularly reinforced-concrete (RC) structures. The design of friction-based dampers is challenging: underestimating the slip force prevents the full use of the potential of the device, which attains the maximum admissible displacement earlier than expected. By contrast, overestimating the slip force may cause delayed triggering of the device when the structure has suffered extensive damage. Therefore, designing the appropriate slip force is an optimization problem. The optimal slip force guarantees the highest inter-story drift reduction. The authors formulated the optimization problem for designing a specific class of friction-based dampers, the asymmetric friction connection (AFC), devised as part of the ongoing multidisciplinary Horizon 2020 research project e-SAFE (Energy and Seismic AFfordable rEnovation solutions). The seismic retrofitting technology involves the external application of modular prefabricated cross-laminated timber (CLT) panels on existing external walls. Friction dampers connect the CLT panels to the beams of two consecutive floors. The friction depends on the mutual sliding of two metal plates, pressed against each other by preloaded bolts. This study determines the optimal slip force, which guarantees the best seismic performance of an RC structural archetype. The authors investigate the nonlinear dynamic response of a coupled mechanical system (RC frame-friction damper) under a set of strong-motion earthquakes, using non-differential hysteresis models calibrated on the experimental cyclic responses. The solution of the optimization leads to the proposal of a preliminary simplified design procedure, useful for practitioners.

1. Introduction

The seismic vulnerability of existing buildings has stimulated the development of non-invasive retrofitting approaches based on passive devices [1–3]. Among them, friction-based dampers have shown great potential when compared with most diffuse-buckling-restrained braces and fluid viscous dampers [4–9]. The performance of friction-based systems is sensitive to the location of the dampers and magnitude of the slip forces. The initial studies on friction dampers focused on experimental tests and technological development of friction-based devices having a rectangular shape of the hysteresis loop [10], such as the slotted bolted connection (SBC) discussed by [11–13]. Lately, several researchers have proposed alternative friction dampers featuring nonrectangular hysteresis curves. Clifton et al. [14] introduced the asymmetric sliding hinge joint (SHJ) for steel moment-resisting frames with nonrectangular hysteresis.

A few studies applied friction devices to timber shear walls. Filiatrault et al. [15] demonstrated the advantage of using friction sliders in timber-sheathed shear walls. Loo et al. [16] replaced the traditional nail plate hold-downs for timber laminated veneer lumber (LVL) walls with symmetric slip friction connections, and confirmed the findings reported by [15]. Hashemi et al. [17] extended the study by [16] to cross-laminated timber (CLT) coupled walls and hybrid timber–steel core walls. Recently, Hashemi et al. [18] developed an innovative, resilient slip friction joint characterized by a nonrectangular hysteresis shape.

The e-CLT technology was developed as part of the ongoing multidisciplinary Horizon 2020 research project e-SAFE (Energy and Seismic AFfordable rEnovation solutions). It entails the application of asymmetric friction connection (AFC) dampers and CLT panels to existing reinforced concrete structures for seismic retrofitting purposes [19].

The AFC is an arrangement of five plates—three steel plates and two thinner plates named shims—assembled using high-strength bolts. The AFCs were studied by [14]. Primary studies on AFCs used brass

* Corresponding authors.
E-mail addresses: angelo.aloisio1@univaq.it (A. Aloisio), francesco.boggian@unitn.it (F. Boggian), roberto.tomasi@nmbu.no (R. Tomasi).

https://doi.org/10.1016/j.engstruct.2021.113807
Received 25 April 2021; Received in revised form 9 August 2021; Accepted 26 December 2021
Available online 21 January 2022
0141-0296/© 2022 The Author(s). Published by Elsevier Ltd. This is an open access article under the CC BY-NC-ND license (http://creativecommons.org/licenses/by-nc-nd/4.0/).

List of symbols

Uppercase Latin

A	Cross-sectional area of CLT panel
E	Longitudinal elastic modulus of timber
G	In-plane shear modulus of CLT panel
$K_{c,\mathrm{sec}}$	Secant shear stiffness of the concrete columns
I	Cross-sectional modulus of inertia of the CLT panel
R	Ratio between the slip load and shear strength of each story
R_{dc}	Displacement capacity of the RC frame
R_{ds}	Displacement capacity of the AFC
S_{dc}	Displacement demand of the RC frame
S_{ds}	Displacement demand of the AFC

Lowercase Latin

a_i, b_i, c_i, q	Parameters of the Atan hysteresis model;
a_g	Seismic acceleration
d	Displacement drift
d_{CLT}	Displacement drift demand variation due to installation of the CLT panel
$d_{\max}$	Maximum displacement drift demand of the e-CLT system
$d_{\max,\mathrm{rc}}$	Maximum displacement drift demand of the RC structure;
d_{optimum}	Displacement drift corresponding to the optimal slip force
$d_s = f_s/k_{\mathrm{clt}}$	Activation displacement of the AFC
d_y	Yield displacement of the RC frame
d_u	Ultimate displacement of the RC frame;
f_{clt}	Resistive force of the CLT panel
f_p	Preload force of each bolt
f_{rc}	Resistive force of the RC frame
f_s	Stable slip force of the AFC
$f_{\mathrm{s,optimum}}$	Optimal slip force
$f_{s,\mathrm{peak}}$	Peak value of the slip force
f_t	Total restoring force of the e-CLT system;
h	Height of the CLT panel
k_{ben}	Bending contribution of the lateral elastic stiffness of the CLT panel
k_{clt}	Lateral elastic stiffness of the CLT panel
$k_{\mathrm{clt},0}$	Lateral elastic stiffness of the CLT panel, tangent value
$k_{\mathrm{clt,sec}}$	Lateral elastic stiffness of the CLT panel, secant value
k_{el}	Lateral elastic stiffness of the CLT panel, related to bending and shear deformability
k_{shear}	Shear contribution of the lateral elastic stiffness of the CLT panel
k_{slid}	Sliding contribution of the lateral elastic stiffness of the CLT panel
$k_{\mathrm{slid},0}$	Sliding contribution of the lateral elastic stiffness of the CLT panel, tangent value
$k_{\mathrm{slid,sec}}$	Sliding contribution of the lateral elastic stiffness of the CLT panel, secant value
m	Lumped mass of the RC frame
n	Number of stories
n_f	Number of AFCs at the ith story
n_p	Number of preloaded bolts
n_s	Number of shear surfaces of the AFC

Lowercase Greek

δ_f	$d_u - d_s$ displacement range of AFC activation
ϵ	Dissipated hysteretic energy
μ	Stable friction coefficient
μ_p	Peak friction coefficient
ξ	Degradation parameter of the AFC
ξ_a, ξ_b	Parameters of the Atan hysteresis model

shims based on the energy dissipation mechanism proposed by [13] for SBCs. The successive studies conducted by [20] extended the concept of the SHJ to mild steel and aluminum shims. Recent studies conducted by [21] introduced shims made of bisalloy grades 80 and 400. The e-CLT technology involves the external application of prefabricated CLT structural panels by connecting them to the RC beams through the AFC (see Fig. 1(a)). When moderate earthquakes occur, the dampers rigidly connect the CLT panels to the RC structure by enhancing the lateral stiffness and strength [22–24]. During strong ground motions, the friction dampers activate with possibly significant energy dissipation. The e-CLT system aims at reducing the story drift demand and damage to nonstructural and structural components. The presented retrofitting intervention may combine the e-CLT technology with nonstructural pre-assembled panels made of wooden frames and replace the existing windows with high-performing windows. Moreover, structural and nonstructural panels integrate bio-based insulation materials and the desired finishing layer to improve the energy performance and architectural image of the renovated building [19]. Cladding solutions integrated to both panels or separated string courses cover the RC beams and protect the dampers while providing the building with architectural uniformity. A decisive feature of the proposed system is retrofitting without interruptions of the building's operational performance.

Fig. 1(b) illustrates an application of this technology to the central bays of an RC building. The e-CLT technology involves the installation of the AFC, the response of which is mostly driven by friction forces. The damper consists of a contacting friction interface clamped by pre-tensioned high-strength bolts: the sliding movement at the friction interface guarantees energy dissipation. The device has two cold-bent steel profiles, which connect the CLT panels of two consecutive stories with the existing interposed RC beam, see Fig. 1(c–d). The upper profile is connected to the RC beam by anchor bolts. The bottom profile is provided with slotted holes and is connected to the upper profile by pre-tensioned high-strength bolts. Standard timber screws connect both the upper and bottom profiles to the CLT panels. The authors report the experimental cyclic response of the considered AFC by addressing the role of the slip force in realizing the optimal design.

To the authors' knowledge, a few studies have focused on the optimal design of friction-based dampers. The most recent studies have examined the optimal design of friction-based dampers installed on structural archetypes through nonlinear dynamic analysis driven by optimization algorithms [26].

Thus far, the most significant achievements related to the optimal design of friction-based dampers are as follows:

- Optimal distribution of the friction device and selection of the optimal slip force value can lead to more than 50% reduction of the inter-story drift of RC frames. Additionally, a non-uniform distribution of the total slip force along the building's height can further reduce the inter-story drift [27,28].

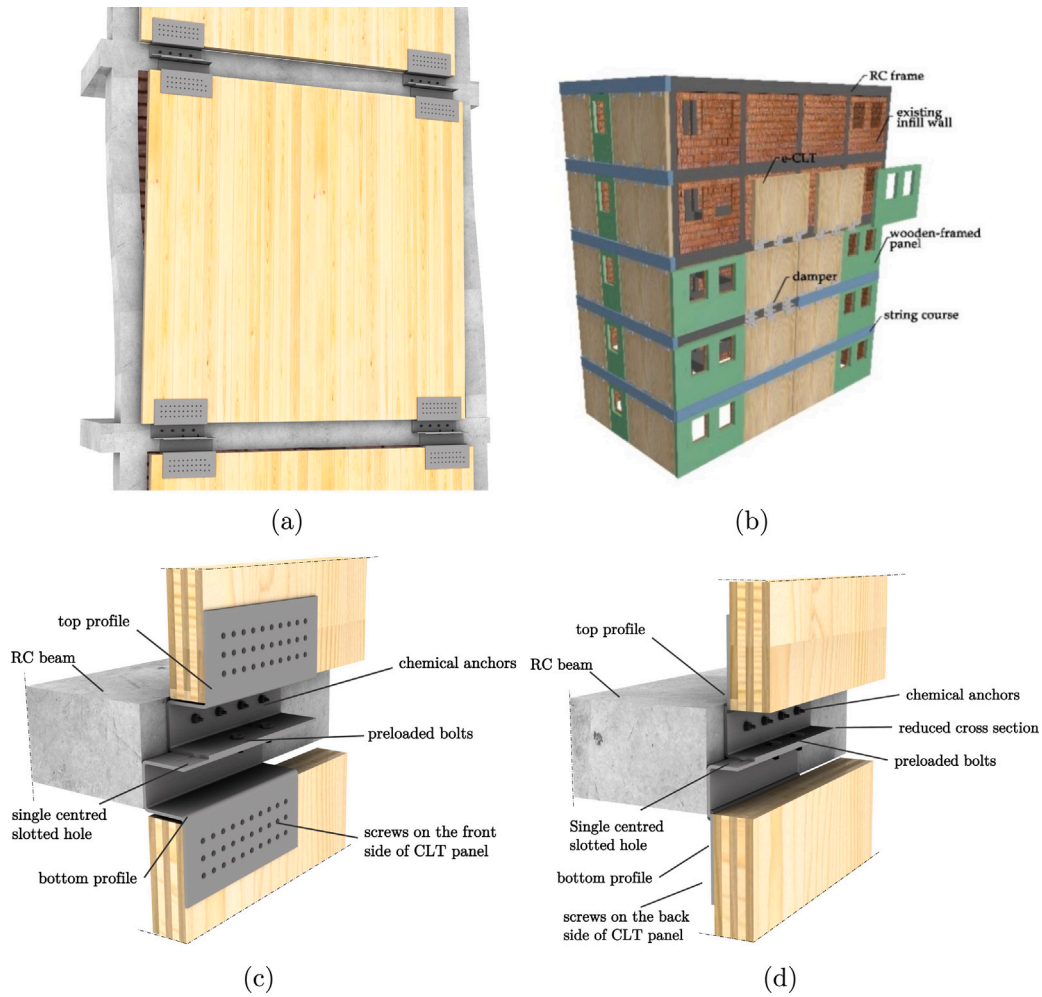

Fig. 1. (a) Proposed friction energy dissipation system; (b) Illustration of a working application; (c) Possible profile design with front-mounted CLT panel; (d) Possible profile design with back-mounted CLT panel.
Source: Modified from [25].

- The optimal slip load values are significantly affected by the amplitude and frequency of the input earthquakes (e.g., peak ground acceleration) rather than the characteristics of the structure [15].
- [29] derived an empirical equation to predict the optimal slip load.

$$R = 1.12\, e^{-0.11n} \tag{1}$$

where R is the ratio between the average of the slip loads with a uniform cumulative distribution and the average shear strength of the stories, and n is the number of stories.

The abovementioned studies, which focused on optimizing the slip-forces in the friction dampers, required extensive parametric studies, which involved modeling a large variety of structural archetypes. However, the main drawback of these analyses was the adoption of simplified constitutive models for concrete and dampers and the modeling of frames without the infill. The use of an elementary Coulomb-like friction model may be inadequate owing to the possibility of a higher slip force during the initial cycles. The stability of the hysteresis loop and magnitude of the friction forces developed by the AFC specimens are directly related to the shim material hardness [30]. The presence of the infill affects the seismic performance of the RC frames significantly by increasing the stiffness and resistance, as well as the ductility and pinching phenomenon [31,32].

This study investigates the performance of the e-CLT technology on an RC frame with masonry infill, which is the primary unit of many existing RC buildings. It does not examine whether providing the cladding for a limited portion of the building, as in Fig. 1b, is adequate for achieving significant seismic mitigation effects. Instead, the study focuses on the response of a single structural unit comprising the RC frame with masonry infill, CLT panel, and AFC. Future research efforts will be devoted to the estimation of the optimal cladding distribution for seismic retrofitting. The following are the novel aspects of the research:

- Discussion of the experimental cyclic response of a novel AFC, included in the e-CLT technology, and presentation of an enhanced Coulomb-like model.
- Investigation of the seismic response of an elementary RC frame equipped with the AFC by using an empirical hysteresis model calibrated on the experimental cyclic response of an RC frame with clay infill. The optimal slip-force in the considered system is estimated, which yields the minimum displacement drift.
- Comparison between the optimization results and existing empirical formulations useful for preliminary design.

The practical significance of this research stands in the proposal of a preliminary design approach of the e-CLT technology based on the results on nonlinear dynamic analysis of the considered structural archetype under different seismic scenarios. The remaining part of this paper is organized as follows. Section 2 describes the response of the

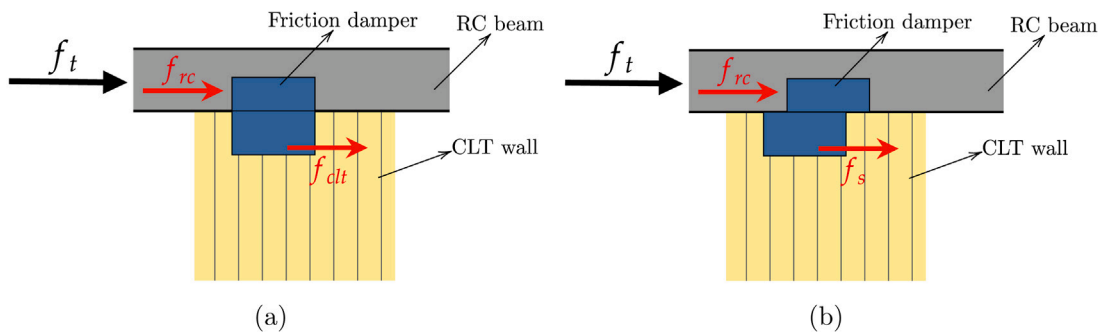

Fig. 2. Illustration of the contributions of forces: (a) before the AFC activation and (b) after the AFC activation.

e-CLT system, Section 3 formulates the optimization problem, and Section 4 describes the experimental tests on friction-based dampers. Section 5 addresses the modeling preferences and calibration of hysteresis models for simulating the RC frame and friction damper. Section 6 discusses the results obtained from the coupled system, and presents the solution of the optimization problem. Section 7 compares the obtained results with the existing formulations by proposing alternative design approaches. The last section draws the conclusions.

2. Mechanical response of e-CLT system

The elementary cell of the e-CLT technology is a parallel structural system. The total resistance f_t is the summation of two contributions, the CLT f_{clt} or the AFC f_s and the RC frame f_{rc}. The level of force attained by the CLT panel drives the condition applicable to the AFC activation, as illustrated in Fig. 2. If the force attained by the CLT panel is below the slip resistance of the AFC, the structural system reflects the summation of the contributions of the RC frame and CLT panel. If the force attained by the CLT panel exceeds the AFC slip resistance, the structural system is the summation of the contributions of the RC frame and AFC.

The governing equations of the considered structural system are as follows:

$$f_t = f_{rc} + f_{\text{clt}} \quad \text{if} \quad |f_{\text{clt}}| \le |f_s| \tag{2}$$

$$f_t = f_{rc} + f_s \quad \text{if} \quad |f_{\text{clt}}| > |f_s| \tag{3}$$

The shear-type system considered here is an elementary mechanical model and does not represent all phenomena related to the coupled system. Finite element (FE) analysis can show the occurrence of local plasticization and coupling phenomena, which are neglected in this formulation. However, the authors selected an elementary analytical mechanical model to carry out multiple nonlinear dynamic analyses with no convergence issues. FE models can grasp the phenomena neglected in simplistic formulations but suffer from stability issues in nonlinear dynamic analysis and are very time-consuming.

The estimation of the design slip force may result in an optimization problem. Fig. 3 illustrates the optimization problem. The elastoplastic constitutive behavior can be considered an elementary representation of the CLT panel equipped with the AFC. A nonlinear backbone expresses the force–displacement response of the RC frame. The design problem results in the estimation of the optimal displacement, derived from the ratio between the slip force and lateral stiffness of the CLT panel.

There are two concurring and opposite trends affecting the seismic performance of the considered structural system.

- An increment in the slip force is proportional to the growth of the hysteretic dissipated energy, displacement demand being equal.
- An increment in the $d_s = f_s/k_{\text{clt}}$ ratio indicates the reduction of the displacement interval associated with the AFC activation, where k_{CLT} is the lateral elastic stiffness of the CLT panel. The AFC can prove its dissipation potential in the displacement range $\delta_f = d_s - d_u$, where d_u is the ultimate displacement of the frame. In Fig. 3, δ_f denotes the displacement interval corresponding to the AFC activation. If the displacement demand exceeds the displacement capacity of the RC frame, the structure has reached the failure condition, and applying the AFC is not beneficial.

The two opposing phenomena reveal the possible existence of an f_s/k_{clt} ratio associated with the optimal seismic performance of the e-CLT system.

3. Design aspects: activation condition

The preliminary design of friction-based dampers is based on the definition of their activation condition. The activation corresponds to the phase when the inertial forces overcome the connection's slip resistance, and the device starts dissipating energy.

The definition of the activation condition is crucial; an early activation may lead to non-optimal use of the elastic energy of the structure. Late activation erodes the safety margin, causing the damper to start dissipating energy when the system has already suffered extensive and critical damage. Therefore, the activation phase must occur just in time to offer maximum benefit to the structure.

It is likely that the activation does not occur simultaneously between all devices, as the structural deformation is not uniform within the structure. Therefore, the optimal design of the activation condition is the most crucial task in designing a retrofitting intervention based on friction dampers. It is necessary to design both the slip force and distribution of the dampers inside the structure.

Let us consider an elementary structural archetype, a plane frame, representing the primary structural unit in an RC frame building. The activation of the dampers at the ith story occurs when the inter-story drift exceeds a given threshold. In the e-CLT technology, the stiffness of each story is the summation of the contributions of the RC frame with the possible participation of the masonry infill, and the CLT panels. The activation occurs when the resistive forces of the CLT walls, associated with a particular inter-story drift d, are equal to the slip forces f_s attained in the n_f dampers installed at that story, as follows:

$$k_{\text{clt}} d = n_f f_s \tag{4}$$

where k_{clt} is the lateral elastic stiffness of the CLT panels. The distinction between the design and known parameters is not straightforward. However, the number of CLT panels per story is fixed, dependent on the number of RC frames without openings. The number of dampers per CLT panel is known due to the limited length of the panel. The stiffness of each story can be estimated from the FE model of the structure, which includes the contribution of the clamped–clamped CLT panels. The design drift d is associated with the device activation and

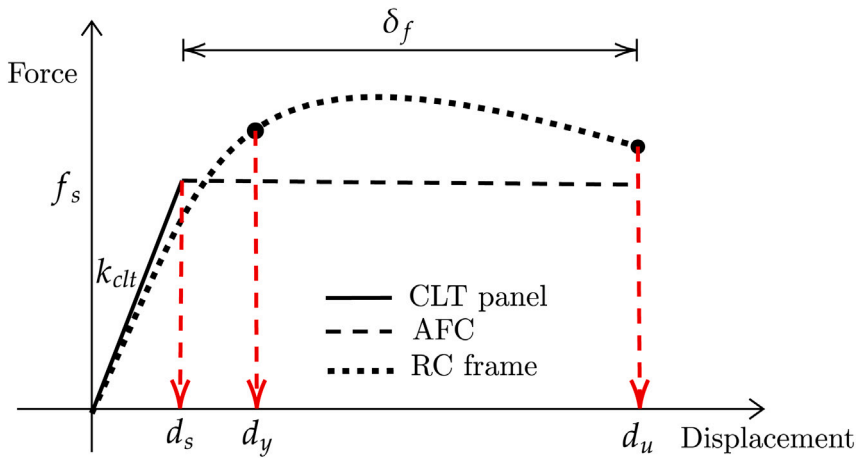

Fig. 3. Qualitative explanation of the design problem: k_{clt} is the in-plane stiffness of the CLT wall, d_y and d_u are the yield and ultimate displacements of the RC frame, d_s is the slip displacement of the AFC, and δ_f is the displacement interval corresponding to the AFC activation.

depends on the balance of the aspects mentioned above. Therefore, d is derived from the evaluations made by the designer based on the expected seismic performance. The design parameters are then the slip force and its distribution within the structure. The choice of the optimal drift to be assumed for the solution of the design problem must ensure the fulfillment of two inequalities:

- The displacement demand of each damper must be lower than its capacity: $S_{d,s} < R_{d,s}$
- The displacement demand of the structure must be lower than its capacity: $S_{s,c} < R_{s,c}$

Nonetheless, the displacement capacity of the structure may be very different from that of the damper, which can endure a large slip, higher than 50 mm. The inter-story drift corresponding to the elastic limit of a shear-type frame in an ordinary RC framed building is of a few millimeters. Therefore, the energy dissipation by the damper must accompany the damage to the structure, when its elastic limit is exceeded. The identity of displacement between the RC frame and dampers imposes the condition that the RC frame must surpass its elastic limit to ensure energy dissipation inside the friction-based device. The dampers cannot prevent but only mitigate the structural damage. Structural plasticization is, therefore, a requirement for the correct functioning of the damper. The energy dissipated within the structural elements as well as that dissipated in the friction damper contributes to the seismic risk reduction.

3.1. Qualitative problem formulation

The authors focus on estimating the slip force associated with the optimal seismic performance of the structural archetype and neglect to determine the optimal distribution of the dampers, which will be considered in future investigations.

Why is the design of the slip resistance a minimum problem? Let us consider the maximum inter-story drift, which is an acknowledged indicator of the damage level in both structural and non-structural elements of RC structures [33]. The inter-story drift is the maximum relative displacement between two adjacent floor levels. The maximum displacement drift demand depends on multiple factors; the authors consider the sole slip resistance of the damper f_s as

$$d_{\max} = f(f_s, \boldsymbol{x}) \tag{5}$$

where $\boldsymbol{x}$ collects the additional variables affecting the maximum drift demand (e.g., structural stiffness). The following paragraphs explain the presumed evolution of the maximum displacement demand $d_{\max}$ as a function of the damper activation displacement $d_s = f_s/k_{\text{clt}}$, qualitatively illustrated in Fig. 4.

The displacement drift is related to the dissipated energy during the seismic excitation. If the damper activation displacement d_s tends to zero, the structure behaves as if no damper is installed.

$$\lim_{d_s \to 0} d_{\max} = d_{\max,rc} \tag{6}$$

where $d_{\max}$ is the maximum displacement demand, and $d_{\max,rc}$ is the maximum displacement demand of the RC structure without dampers. If the damper activation displacement d_s tends to infinity (Eq. (7)), the damper does not activate, and the structure behaves as if the damper acts as a rigid connection between the RC beam and timber panel. Thus, the CLT panel behaves as an additional stiffening element reducing the maximum displacement demand; the slip resistance is higher than the shear resistance of the RC structure, denoted by the double vertical line in Fig. 4.

$$\lim_{d_s \to \infty} d_{\max} = d_{\max,rc} - d_{CLT} \tag{7}$$

where d_{CLT} is the reduction in the displacement demand due to the additional stiffness of the CLT panel. If the slip resistance increases from zero, as in Fig. 4, the dissipated energy increases. The damper activates when there are low inertial forces. Nevertheless, the friction-based device must endure significant displacement to obtain reasonable energy dissipation. However, the drift should reduce, and the following derivative would be negative:

$$\lim_{d_s \to 0} \frac{\partial d_{\max}}{\partial d_s} < 0 \tag{8}$$

If the slip force is lower than the shear resistance of the structure, the damping device is activated, as shown by the green region in Fig. 4. However, if the slip resistance becomes lower than the shear resistance of the RC frame (red area in Fig. 4), the expected drift would reduce. The damper may start dissipating energy before the system attains the maximum displacement capacity, thus increasing the dissipated energy and possibly lowering the drift demand. The AFC has larger displacement margin for dissipation. Therefore, the following derivative would be positive:

$$\lim_{d_s \to d_u} \frac{\partial d_{\max}}{\partial d_s} > 0 \tag{9}$$

where d_u is the ultimate displacement of the RC frame. The design of the slip force resembles a minimum problem. It is likely that a force value exists, which may minimize the drift demand during seismic excitation. The mathematical problem cannot have a closed-form formulation. The optimal performance depends on the expected seismic scenario. Therefore, the authors followed an *a posteriori* approach,

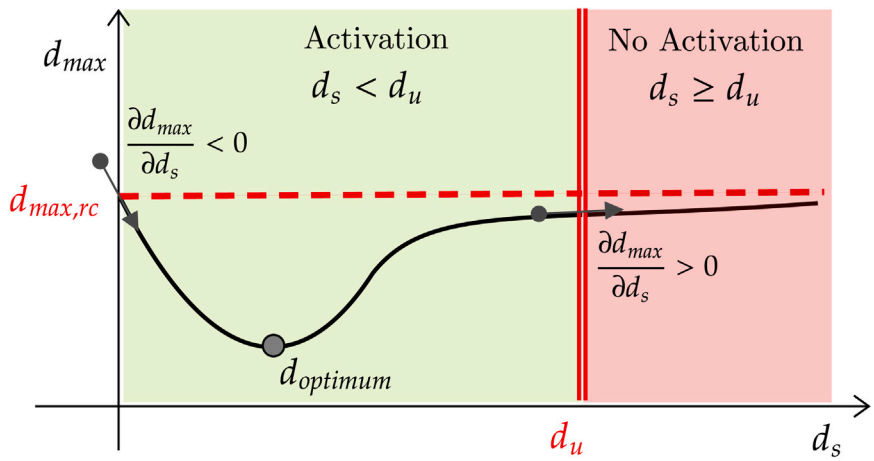

Fig. 4. Qualitative illustration of the trend of the maximum displacement $d_{\max}$ as a function of the damper slip displacement d_s. (For interpretation of the references to colour in this figure legend, the reader is referred to the web version of this article.)

which is a conventional approach in earthquake engineering. They selected a set of earthquakes matching the given design spectrum. Then, they estimated the nonlinear dynamic response of a specific structural archetype by varying the slip resistance within a given range; the minimum of these values obtained from the considered list of earthquakes leads to the optimal solution.

$$f_{s,\text{optimum}} = \arg\min_{f_s} d_{\max}(f_s, a_g) \tag{10}$$

where a_g represents a seismic scenario. This study aimed to solve the minimum problem in a specific structural configuration representing the anatomical unit of the e-CLT technology.

4. Experimental tests

The authors investigated the cyclic behavior of the AFC devised for the e-CLT technology. The considered setup focuses on the friction damper and does not include the CLT elements (see Fig. 6). The prototype was fabricated from 8 mm cold-bent S235 steel plates. The specimen had an overall width of 450 mm, height of 325 mm, and depth of 105 mm, approximately equal to the commercial thickness of a CLT panel (100 mm). The prototype consisted of a couple of plates with different holes. Two designs are shown in Fig. 1(c) and (d). The "top" profile has holes for connections with the RC beam and round holes on the interface surface with the "bottom" profile. The bottom profile has slotted holes, which guarantee the sliding between the two profiles and host preloaded bolts. The clearance of movement is 100 mm in each direction, plus some tolerance. Both profiles have holes in the outer plates for screwed connections with the CLT panels.

The preliminary testing campaign was aimed at studying and isolating the friction behavior. The specimen was tested within a rigid steel frame with 100 × 200 mm rectangular section columns of 12.5 mm thickness. The bottom profile of the specimen was attached to the right column, and the top profile, reduced to a C-shape for testing purpose, was in the central part of the frame and was free to slide, being connected to the actuator of the press. The top element was moved up and down by the press machine, to simulate the RC beam movement in a real building. The choice of the slip surface on the horizontal rather than the vertical plane depends on the expected behavior of an RC building, characterized by the prevalent shear-type response. An additional steel cap plate and two aluminum shim layers were inserted between the profiles to obtain an asymmetrical friction connection, as described by [34]. The authors selected an aluminum shim because of its good friction stability when compared with steel vs. steel friction, as observed by [30], and owing to its ease of manufacture and supply when compared with other high-hardness alloys. In this study, the authors did not address the effect of long-term issues related to device degradation. In addition, the surface did not receive any treatment to simulate the degradation phenomenon. The bottom profile was fixed to the column, in place of the CLT panel used in practical applications. The two profiles were clamped together by two 10.9 class M14 EN14399 bolts [35], which were preloaded by following the torque method described in [36]. Fig. 5 shows the components of the tested specimens. The authors tested different geometries and configurations of the connectors; a complete description of the entire testing process can be referred from [37,38]. The scope of this paper is not to present the complete experimental setup, but to focus on the specimen exhibiting the expected behavior after the initial trials, as this was used as the basis for generating the model by using network linear discriminant analysis (NLDA). The loading protocol was cyclic, adapted from ISO16670 [39] and EN15129 [40], which express the protocol as a function of the ultimate displacement. In this case, the test was displacement driven at a speed of 2 mm/s and the cycles were 1 × 5 mm + 3 × 10–20–30–40–50 mm. The load was measured by using the press load cell, and the displacement of the top profile was recorded using both the press and an additional wire sensor. Two horizontal LDTs acquired the displacement measurements at the top and bottom of the right column to prove the sufficient stiffness of the setup. The goal for the friction connection in the current setup is to obtain a 30 kN sliding force; this threshold depends on the operational limit of the press machine and previous FEM models [25]. The preload force in the bolt was set to $f_p = 36$ kN, which resulted in an experimental slip resistance of $f_s = 29.57$ kN, calculated as in [16]. Fig. 7 also shows the result in terms of loops, force, and dissipated energy. The experimental friction coefficient is calculated as

$$\mu = \frac{f_s}{n_s n_b f_p} = \frac{29.57}{2 \cdot 2 \cdot 36} = 0.21 \tag{11}$$

where f_s is the experimental slip resistance, $n_s = 2$ is the number of shear surfaces, $n_b = 2$ is the number of the preloaded bolts, and f_p is the preload force in the bolts. Interestingly, the estimation of the resistant slip force is not straightforward. The hysteresis loop does not display a perfectly rectangular shape. There is a significant increment in the slip resistance in the first few cycles at lower displacements, whereas it stabilizes at higher displacements to an almost constant value equal to 30 kN. This effect is not negligible, as there is an approximate 56% increment in the peak-to-stable value at higher deformations. The modeling of this phenomenon is mandatory to achieve a reliable prediction of the performance of this system.

This aspect is in full accordance with the experimental tests reported by [30]. Specifically, employing an aluminum plate, characterized by

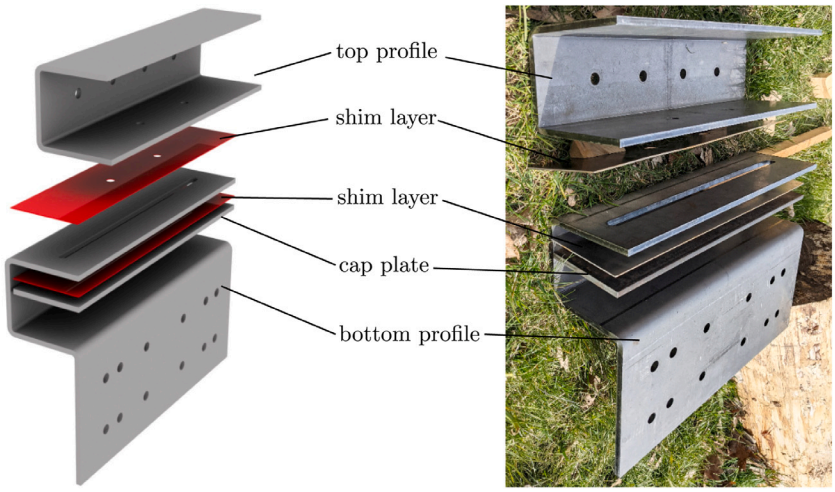

Fig. 5. Illustration and photographs of the parts of the specimen.

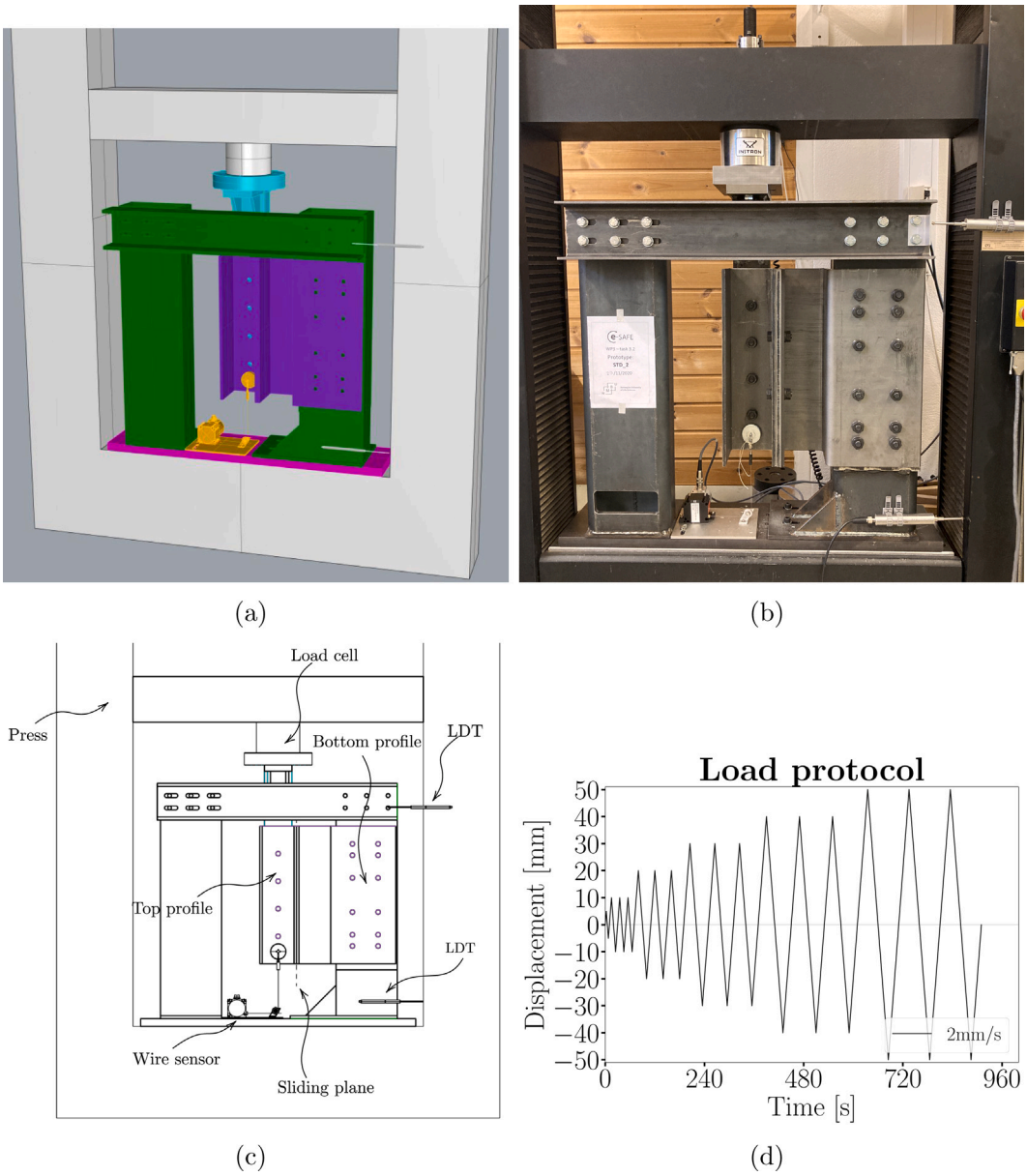

Fig. 6. (a) 3D model of the setup; (b) Setup with all measuring instruments mounted; (c) Illustration of the setup; (d) Loading protocol.

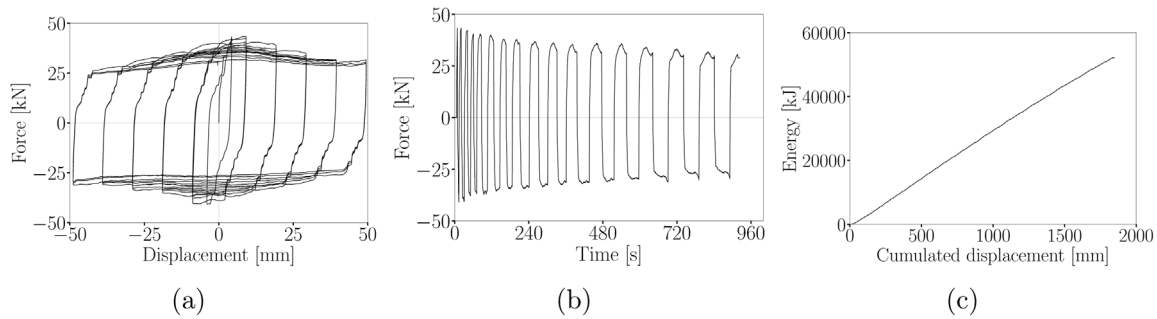

Fig. 7. (a) Experimental hysteresis loop; (b) Force–Time function; (c) Dissipated energy–cumulated displacement function.

low hardness, causes moderately stable loops. The friction coefficient corresponding to the peak force value is

$$\mu_p = \frac{f_{s,peak}}{n_s n_b f_p} = \frac{47.03}{2 \cdot 2 \cdot 36} = 0.33 \tag{12}$$

where $f_{s,peak}$ is the peak value of the slip force. This value is in accordance with the findings by [30], who obtained a static friction coefficient of 0.34 and dynamic friction coefficient of 0.21 in the case of aluminum shims. Accurate modeling of AFC may require energy-dependent modeling of the friction coefficient. The friction coefficient does not depend on the displacement drift attained by the sliding bolts: Fig. 7 shows that there are different slip forces for the same displacement value. Conversely, the dissipated energy, which is always increasing, may represent a valid parameter for the proper modeling of the μ variability.

5. Calibration of hysteresis models of friction damper and RC frame

The e-CLT technology primarily addresses the seismic retrofitting of existing RC structures. Most of the traditional RC buildings possess masonry infill. An infill with a regular in-plane and elevation distribution produces a beneficial effect. The proper design of the coupled response of an AFC and RC frame requires predicting the infill effect of the masonry infill. It generally causes a gain in the strength and stiffness. An estimation of the optimal slip force on an RC frame without infill may cause a dangerous underestimation of the activation condition to achieve the expected benefits. Therefore, rather than relying on elementary modeling of the infill by using an equivalent diagonal strut, the authors favored the modeling of the cyclic response of an RC frame by using an empirical hysteresis model calibrated on experimental data. The authors adopted the experimental data of [31] for an RC frame with clay masonry infill, typical of ordinary RC buildings. The authors did not address the variance related to the high uncertainty of the RC infill frame. Therefore, the authors preferred to focus on real case studies by adopting empirical hysteresis models of both the AFC and RC frame. The following subsections describe the hysteresis models used for mirroring the hysteretic response of the considered RC frame and the tested AFC. The last part examines the hysteretic response of the coupled system, obtained by assembling the AFC and RC frame.

5.1. Modeling of the RC frame

The authors modeled the hysteretic response of the RC frame, as shown in Fig. 8(a). Fig. 8(b) shows the experimental cyclic response by increasing the displacement at each cycle up to a drift of 2.5%. The increment in the cycle amplitude was unsteady while loading up to a maximum of 10 mm in the last cycles. The response exhibits a prominent pinching behavior with progressive decay in strength and stiffness.

The authors reproduced the hysteretic response in Fig. 8(b) by using the Atan model, proposed by [41], which suits the simulation of mechanical systems with pinching, and strength and stiffness degradation.

Table 1
Parameters of the Atan model for the simulation of the cyclic response of the RC frame in Fig. 8.

Parameter	Value
a_0	140.12
$b_{0,1}$, $b_{0,4}$	0.71
$b_{0,2}$, $b_{0,3}$	0.32
$b_{0,5}$, $b_{0,6}$	0.25
c_{1-6}	0.20
ξ_{ai}, ξ_{bi}	0.00005
q	0.80

It is a hysteresis model based on the arctangent function characterized by the piecewise definition in Eq. (13), where the six conditional statements identify the transition between the different parts of the hysteresis. A set of three parameters define the arctangent function in each section of the loop: a_i denotes the amplitude of the force, b_i is the x-axis resolution, and c_i is the residual displacement. The subscript i varies between 1 and 6. The strength and stiffness degradation are described by an exponential function, as in [42,43]. The exponential function expresses the force and stiffness degradation as a function of the dissipated hysteretic energy (ϵ). The energy-dependent definitions of a_i and b_i are

$$a_i(\epsilon) = e^{(-\xi_{a_i}\epsilon)} a_0 \tag{14}$$

$$b_i(\epsilon) = e^{(-\xi_{b_i}\epsilon)} b_{0,i} \tag{15}$$

where ξ_{a_i} and ξ_{b_i} are properly calibrated to the degradation of the strength and stiffness, respectively. The parameters are $a_0 = \frac{2F_u}{\pi}$ and $b_{0,i} = \frac{k_{0,i}}{a_0}$, where $k_{0,i}$ is the tangent stiffness, and F_u is the ultimate resistance.

Fig. 8(c) displays the superposition between the experimental cyclic response of the RC frame and the simulated response using the Atan model with the parameters in Table 1. The model satisfactorily follows the experimental data by exhibiting the expected degradation behavior. The significant stability of the model under dynamic excitation endorsed the adoption of this formulation: it was especially conceived to enhance the stability of hysteresis models with pinching, which suffer from several convergence issues due to the stiffness boost in the pinched branches.

5.2. Modeling of the friction damper

Columbian friction mainly drives the cyclic response of the AFC. Therefore, the authors adopted the following definition of the slip force:

$$f_s(\epsilon) = \mu(\epsilon) f_p \,\mathrm{sign}(\dot{d}) \tag{16}$$

where $f_s(\epsilon)$ is the slip force, f_p is the absolute value of the preload force, $\dot{d}$ the velocity of deformation, and ϵ is the dissipated hysteretic

$$f_{rc} = \begin{cases} a_1 \arctan(b_1 x - |c_1|) & \text{if} \quad \{\dot{x} > 0,\ x > 0,\ |x| > q \max(|x(t)|) \forall t \in [0, t)\} \\ a_2 \arctan(b_2 x - |c_2|) & \text{if} \quad \{\dot{x} < 0,\ x > 0\} \\ a_3 \arctan(b_3 x + |c_3|) & \text{if} \quad \{\dot{x} < 0,\ x < 0\} \\ a_4 \arctan(b_4 x - |c_4|) & \text{if} \quad \{\dot{x} > 0,\ x < 0,\ |x| > q \max(|x(t)|) \forall t \in [0, t)\} \\ a_5 \arctan(b_5 x + |c_5|) & \text{if} \quad \{\dot{x} > 0,\ x < 0,\ |x| \le q \max(|x(t)|) \forall t \in [0, t)\} \\ a_6 \arctan(b_6 x + |c_6|) & \text{if} \quad \{\dot{x} > 0,\ x > 0,\ |x| \le q \max(|x(t)|) \forall t \in [0, t)\} \end{cases} \tag{13}$$

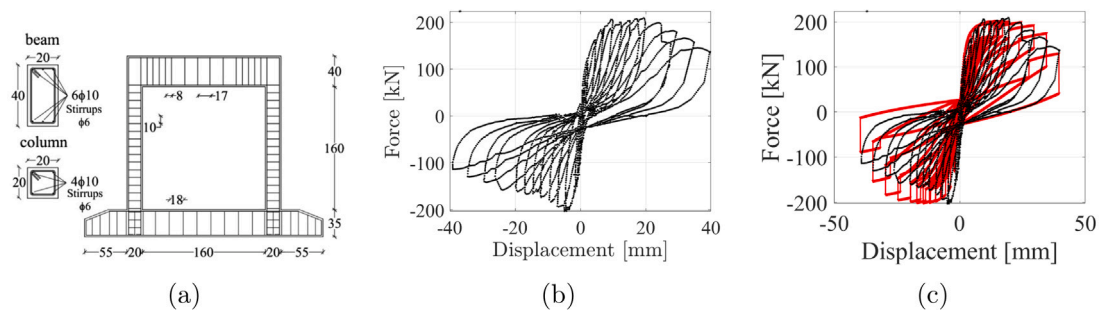

Fig. 8. (a) RC frame subject to cyclic loading based on [31]; units of dimensions: cm, units of rebar diameter: mm; (b) Experimental hysteresis loop; (c) Comparison with the Atan model.

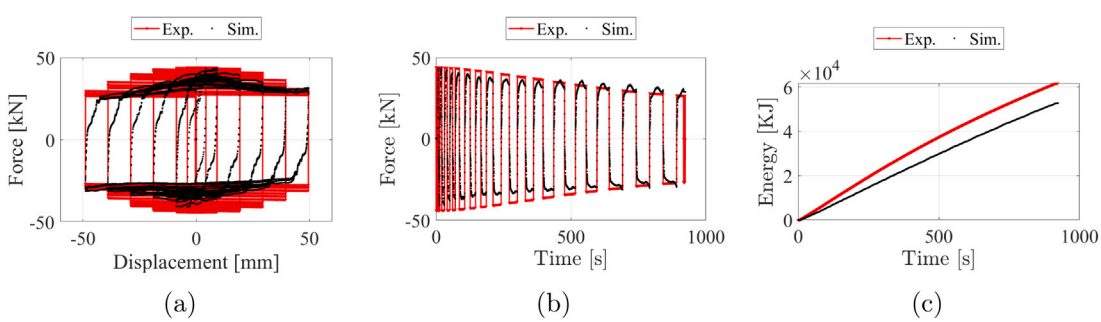

Fig. 9. Comparison between experimental data and Coulomb-like friction model: (a) Hysteresis loop; (b) Force–Time function; (c) Dissipated energy–time function.

energy. The definition of the friction coefficient is

$$\mu(\epsilon) = \mu_0 \left[\exp(-\xi\epsilon) + 1\right] \tag{17}$$

where μ_0 and ξ from an ordinary least squares optimization are 0.33 and 0.00005, respectively.

The authors noticed that an exponential function closely follows the strength evolution of the AFC. Fig. 9 shows the comparison between the experimental data and the Coulomb-like friction model. The model reproduces the experimental response, but it exhibits energy dissipation higher than expected due to the loop's non-rectangular shape, caused by the corner chipping effect. The inversion of the velocity sign does not cause a vertical transition between the positive and negative values. After an initial vertical drop, the transition becomes smoother with increase in the slip value. This effect causes lower energy dissipation, as evidenced in Fig. 9(c). The authors neglect this phenomenon in the current investigation owing to its limited influence on the dissipated hysteretic energy. Structural models are generally conservative. However, the dissipated energy overestimation can be considered negligible for engineering purposes. Furthermore, the proposed rigid-plastic model might lead to higher acceleration due to abrupt change in stiffness. However, the elastic branch connecting the axis origin to the plastic branch has a high slope, as evidenced by the experimental data. Therefore, the authors believe that a rigid-plastic model could be a good approximation in engineering-oriented simulations.

5.3. Modeling of the CLT panel

Following the standard approach in structural engineering, the authors assumed an elastic behavior of the CLT panel up to the ultimate force value, where the lateral elastic stiffness of the CLT panel was equal to the secant value: $k_{\text{clt}} = k_{clt,sec}$.

In the e-CLT system, the CLT panel should not reach the full plasticization of the connections. The panel should not experience extensive damage, and the dissipation should be localized in the AFC. Consequently, the authors modeled the CLT panel with an equivalent elastic spring, as follows:

$$f_{\text{clt}} = k_{\text{clt}} d \tag{18}$$

where f_{clt} is the resistive force of the CLT panel, k_{clt} is the lateral elastic stiffness, and d is the horizontal displacement.

The analyses are valid until the attainment of the ultimate force of the CLT panel. If the total resistive force exceeds the CLT panel resistance, the e-CLT system does not exhibit proper functioning, and it is not worthy of further consideration.

The correct choice of k_{clt} is crucial. In the next paragraphs, the authors report a few considerations, which led to the selection of a possibly reliable value of k_{clt}.

In the e-CLT system, the CLT panel is constrained on both sides by AFCs and by fixed connectors to the RC beam. As depicted in Fig. 10, the constrained arrangement does not allow the rotation of the panel and the consequent rocking motion typical of CLT shear

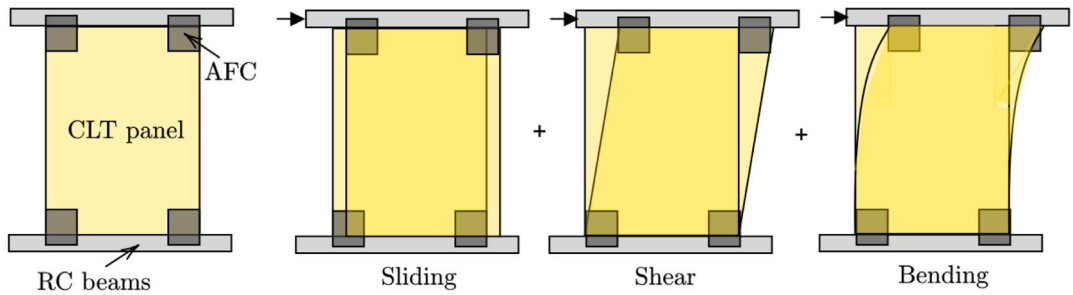

Fig. 10. Qualitative explanation of CLT panel response.

Table 2
Characteristics of the tested CLT shear walls.

Specimen CLT	STD	NA620	ND620	NA340	NAWH
Sliding restraint	100CR	10060newA	10060newD	10060newA	10060newA
n°	3	3	3	3	3
Fastener type	Anker nails	Anker nails	Anker nails	Anker nails	Anker nails
n°	12	30	30	30	30
ø [mm]	4	4	4	4	4
l [mm]	60	60	60	60	60
Uplift restraint	WHT340	WHT620	WHT620	WHT340	/
n°	2	2	2	2	/
Fastener type	Anker nails	Anker nails	Anker nails	Anker nails	/
n°	20	52	52	20	/
ø [mm]	4	4	4	4	/
l [mm]	60	60	60	60	/

walls. Therefore, the three possible deformations are panel sliding, elastic bending, and shear deformation. The sliding motion depends on the horizontal stiffness of the connections. However, although the elastic lateral stiffness of a clamped–clamped panel with no sliding can be straightforwardly predicted from the elasticity theory, the sliding contribution depends on the arrangement, number, and typology of the connections. Eq. (19) provides the lateral elastic stiffness of a clamped–clamped beam with banding and shear deformability:

$$\frac{1}{k_{\mathrm{el}}} = \frac{1}{k_{\mathrm{ben}}} + \frac{1}{k_{\mathrm{shear}}} = \frac{1}{\frac{12EI}{h^3}} + \frac{1}{\frac{GA}{1.2h}} \tag{19}$$

where k_{el} is the lateral elastic stiffness of the CLT panel, related to bending and shear deformability, k_{ben} is the bending contribution of the lateral elastic stiffness of the CLT panel, k_{shear} is the shear contribution of the lateral elastic stiffness of the CLT panel, h is the height of the panel, E is the longitudinal elastic modulus, I the cross-sectional inertia, G is the shear modulus, and A is the cross-sectional area. Under actual circumstances, the clamped–clamped configuration is arduous to achieve, and the connection deformability may affect the lateral stiffness of the CLT panel.

The authors examined the effect of sliding deformation on the lateral stiffness by discussing the selected results from the cyclic tests on the CLT wall panels, presented by [44] and detailed in Table 2.

The considered panels present the number of base connections compatible with a possible connection layout of the e-CLT system, and can be used to derive the possible range of variation of the sliding stiffness.

The tested CLT shear walls, loaded according to the EN 12512 protocol [45], had the following characteristics: size 250 × 250 cm, and three layers (thickness 30–30–30 mm) of C24 boards. Different vertical loads (L0, L10, L20 indicate the vertical distributed load in kN/m, respectively) and various connections to the ground formed the basis for a comparative assessment between the specimens—precisely, three types of angle brackets, two types of hold-down, and a specimen without hold down. The considered CLT panels had base constraints and were free to rock. Therefore, it was possible to determine the sliding response, which depended on the base connections, from the displacement measurements at point D (see Fig. 11(a)). The sliding motion depends on the timber–connection interaction and the connection layout reported in Table 2.

Fig. 11(b) plots the resistive force vs. sliding motion of the STD-L20 CLT panel. The elastic stiffness of a clamped–clamped CLT panel is approximately 33 kN/mm, using the parameters E = 11600 MPa and G = 450 MPa [46]. Interestingly, there was no significant difference between the lateral elastic stiffness of the clamped–clamped CLT panel and the secant stiffness due to sliding, which was approximately equal to 11.16 kN/mm for the STD-L20 sample. The secant stiffness is obtained from the intersection between the axes origin and the maximum force value. Table 3 proves that the lateral stiffness of the panel due to sliding deformation is similar to the lateral stiffness due to bending and shear, estimated from Eq. (19). In a serial system, where the total displacement is the summation of the sliding, bending, and shear deformation components, the equivalent stiffness is expressed as

$$\frac{1}{k_{\mathrm{clt}}} = \frac{1}{k_{\mathrm{slid}}} + \frac{1}{k_{\mathrm{shear}}} + \frac{1}{k_{\mathrm{ben}}} \tag{20}$$

where k_{clt} is the lateral elastic stiffness of the CLT panel, whereas k_{slid}, k_{bend}, and k_{shear} are the lateral stiffness contributions associated with the sliding, bending, and shear deformation, respectively. Table 3 lists the obtained lateral stiffness values of the CLT specimens from Eq. (20) by using the secant and tangent stiffness values estimated from the experimental data and the elastic stiffness from Eq. (19). The stiffness values do not manifest significant variability. In this paper, the authors adopted the mean value based on the secant stiffness of the CLT panel, as follows:

$$k_{\mathrm{clt}} = 13 \text{ kN/mm} \tag{21}$$

In conclusion, the correct design of the CLT panel entails an accurate estimation of the secant stiffness and ultimate resistance of the CLT panel in the chosen connection arrangement. In this study, the authors derived the general rules of design of the e-CLT and did not assume a specific connection arrangement.

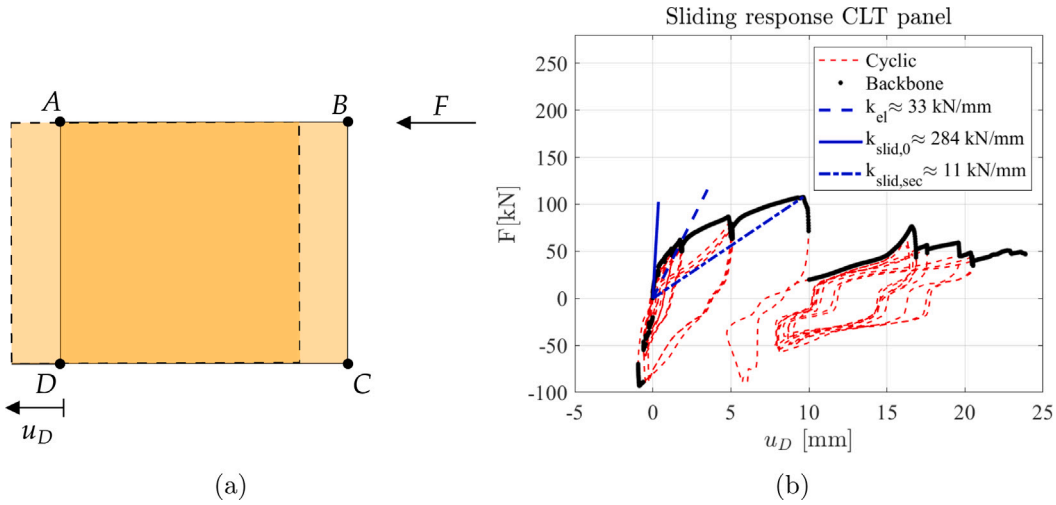

Fig. 11. Displacements field of the wall and (b) hysteresis curve in terms of horizontal force in B (F) and horizontal sliding (u_D).

Table 3
Tangent $k_{slid,0}$ and secant stiffness $k_{slid,sec}$ of the force-sliding hysteresis curves of the CLT specimens detailed in Table 2; elastic stiffness k_{el} of the CLT specimens from Eq. (19); lateral elastic stiffness of the CLT panel from Eq. (20) by using the secant $k_{clt,sec}$ and tangent $k_{clt,0}$ sliding stiffness values.

Specimen	$k_{slid,0}$ [kN/mm]	$k_{slid,sec}$ [kN/mm]	k_{el} [kN/mm]	$k_{clt,0}$ [kN/mm]	$k_{clt,sec}$ [kN/mm]
STD-L0	42.12	6.11	33.00	18.50	5.16
STD-L20	284.90	11.16	33.00	29.57	8.34
NA620-L0	11.52	35.85	33.00	8.54	17.18
NA620-L20	189.77	51.29	33.00	28.11	20.08
ND620-L0	110.44	28.52	33.00	25.41	15.30
NDS20-L20	181.39	43.80	33.00	27.92	18.82
NA340-L20	354.33	34.73	33.00	30.19	16.92
NAWH-L20	27.71	4.40	33.00	15.06	3.88
Mean	150.27	26.98	33.00	22.91	13.21

6. Results

The inelastic restoring force in Eqs. (2)–(3) contributes to the equilibrium of a single-degree-of-freedom oscillator (SDOF), which is representative of the dynamic response of the RC frame. The analysis focuses on the behavior of the structural unit of the e-CLT system by neglecting all aspects related to the practical scenario of a full-size building (e.g., the effect of the added mass of the e-CLT, higher mode effects, and slip optimization along with height of the structure). The equilibrium of a lumped mass above the frame yields the following ordinary differential equation (ODE) under earthquake excitation:

$$m\ddot{x} + f_t = -m\ddot{x}_g \tag{22}$$

where m is the mass equal to 20 t, x is the displacement, $\ddot{x}$ is the double derivative of x with respect to time, f_t is the resisting inelastic force defined in Eqs. (23)–(24), and $\ddot{x}_g$ is the ground acceleration.

$$f_t = f_{rc} + f_{\text{clt}} \quad \text{if} \quad |f_{\text{clt}}| \le |f_s| \tag{23}$$

$$f_t = f_{rc} + f_s \quad \text{if} \quad |f_{\text{clt}}| > |f_s| \tag{24}$$

Eqs. (18), (16), and (13) describe the f_{clt}, f_s, and f_{rc} terms, respectively. The authors solved Eq. (22) in MATLAB. A SDOF system is the most elementary archetype. Nonetheless, assessing its behavior is the basis for achieving a complete understanding of the response of multiple-degrees-of-freedom systems. The SDOF model is used to assess the slip force, which guarantees the lowest inter-story drift. An RC frame represents any story distinguished by a prevalent shear-type response. Any structure can be considered a standalone case, but the accurate analysis of an elementary model enables a careful assessment of the optimal ranges to be expected in structures of greater complexity. In contrast with the previous section, the displacement is unknown and must be derived from the numerical integration of the ODE. The authors used the explicit fourth-order Runge–Kutta method for the temporal discretization of the approximate solution of the ODE.

Figs. 12–13 show the responses of the SDOF oscillator without and with the AFC (f_s = 20 kN) to the El Centro earthquake. The two figures provide qualitative information and will be followed in the next section by more extensive simulations for a large set of strong-motion earthquakes. The displacement time–history demonstrates the displacement drifts and plasticization phenomenon in both systems. However, the absolute value of the displacement drift reduces with the AFC. Nearly 50% reduction is observed, from approximately 4 mm to 2 mm. Although the force values are very similar, the displacement reduces. The hysteresis loops further prove the gain in dissipated energy: the loop of the system with AFC expands to that without it.

The simulated pseudo-static test of the considered system with AFC revealed a 22% increment in the dissipated energy when compared with the RC infilled frame. Thus, the authors expect to observe beneficial effects in regard to the drift demand reduction from nonlinear dynamic analyses. The advantage of the AFC cannot be estimated from the force-based analysis. The primary benefit arises from the displacement response.

6.1. Results: Optimization of slip force

The optimization of the slip force in the AFC stems from an indirect approach. The authors simulated the response of an RC frame equipped with the AFC to a set of 41 earthquakes by varying the value of the slip force in a given range. A list of 41 Italian earthquake records with magnitude M_L ranging between 5 and 6.5, as presented in Table 4, represented the base for generating 41 artificial earthquakes,

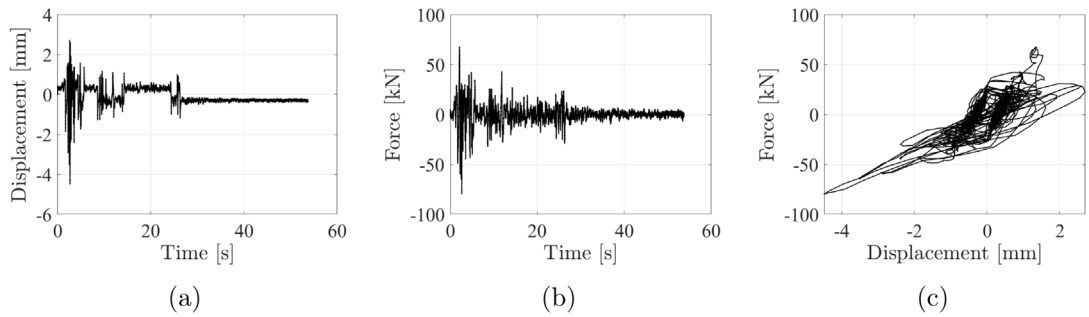

Fig. 12. Response of the RC frame to the El Centro earthquake: (a) Displacement time–history; (b) Force time–history; (c) Force–Displacement data.

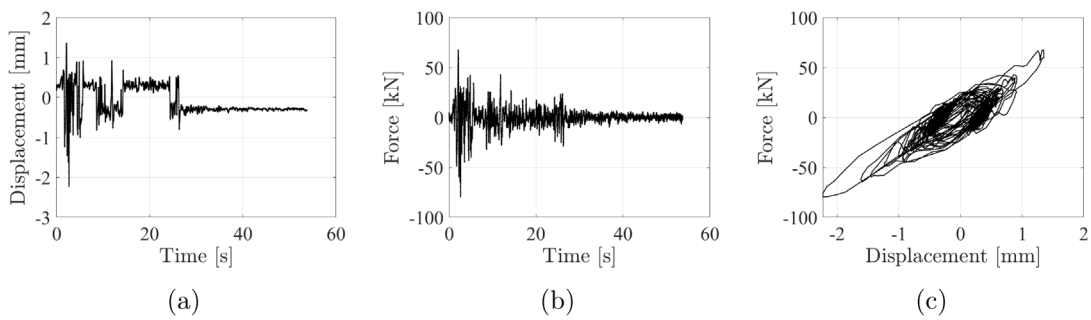

Fig. 13. Response of the RC frame equipped with the friction damper to the El Centro earthquake: (a) Displacement time–history; (b) Force time–history; (c) Force–Displacement data.

scaled to the same peak ground acceleration (PGA) and optimized to match the design spectrum in Fig. 14. The design spectrum corresponds to the seismic scenario expected in L'Aquila, Italy, according to the National Seismic Code [47]. The algorithm proposed by [48] is used to scale the accelerograms and carry out the analyses based on coherent inputs (see Fig. 14). The algorithm modifies the frequency content without producing substantial shape modifications. Fig. 14 shows the pseudo-acceleration response spectrum. The superposition of the response spectra of the considered set appears around the design spectrum, marked by a solid red line. The force slip varied in the range of 0–100 kN, in steps of 1 kN. Fig. 15 displays the results of the analyses. Fig. 15(a) reports the maximum displacement drift due to a single earthquake. The maximum inter-story drift is widely used to evaluate the level of damage to both structural and non-structural elements in RC structures [33]. Fig. 15(b) superposes the curves in Fig. 15(a) by considering the responses to the 41 earthquakes. The mean and variance of the minima of the curves in Fig. 15(b) leads to the normal distribution shown in Fig. 15(c), where the result is that the optimal value of slip force is $f_{s,\text{optimum}} = 45$ kN.

The curves do not exhibit a smooth trend: they are very jagged. The "saw-tooth" variations in drift demand are possibly caused by the nonlinear dynamic coupling between the seismic input and the time-variant structural features. However, despite the oscillation, each curve has a range of minima with a concave shape. Hence, the authors picked the argument corresponding to the lowest value, which is considered representative of the optimal slip force. There are considerable differences between the curves obtained from different earthquakes. This evidence agrees with the findings by [15] who observed that the optimal slip load values are more affected by the amplitude and frequency of the input earthquakes (e.g., peak ground acceleration) than the structural characteristics.

Interestingly, the range of local minima gathers at the lower values of the slip force.

In addition, [29,49], and [50] observed that the use of friction dampers is associated with a range of optimal slip load ratios, leading to a significant lower inter-story drifts. According to [29], the slip load ratio is the ratio between the slip value and the resistance of

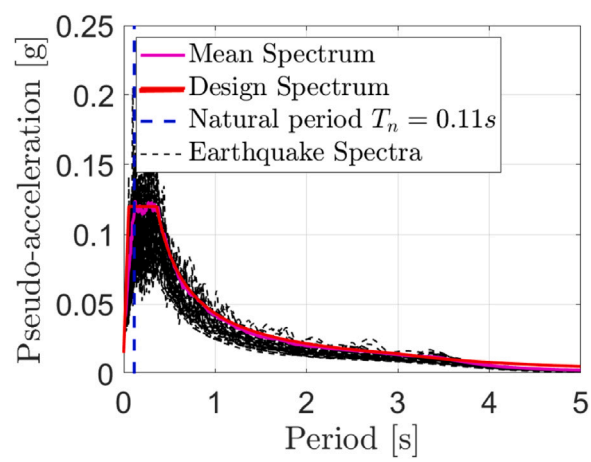

Fig. 14. Pseudo-acceleration response spectrum. (For interpretation of the references to colour in this figure legend, the reader is referred to the web version of this article.)

the structure without the passive device. They found the following empirical function for the prediction of the optimal slip force as a function of the number of stories n:

$$R = 1.12e^{-0.11n} \tag{25}$$

In the case of a single story, the R ratio is almost one. As the number of stories increases, the R ratio reduces to 0.12. This empirical equation does not agree with the outcomes of this investigation. The R ratio in the considered configuration is $R \approx 0.23$, for $f_{s,\text{optimum}} = 45$ kN.

According to [29], in the considered case, the optimal slip resistance should be approximately equal to 200 kN. Numerous factors affect the optimal value of the slip force. Both the RC frame and the AFC dissipate the seismic energy. The energy dissipated by the friction dampers is proportional to the slip force and the mutual drift. If the slip force is kept low, the increment in the dissipated energy depends on the increment in the displacement. If the slip force is higher, a

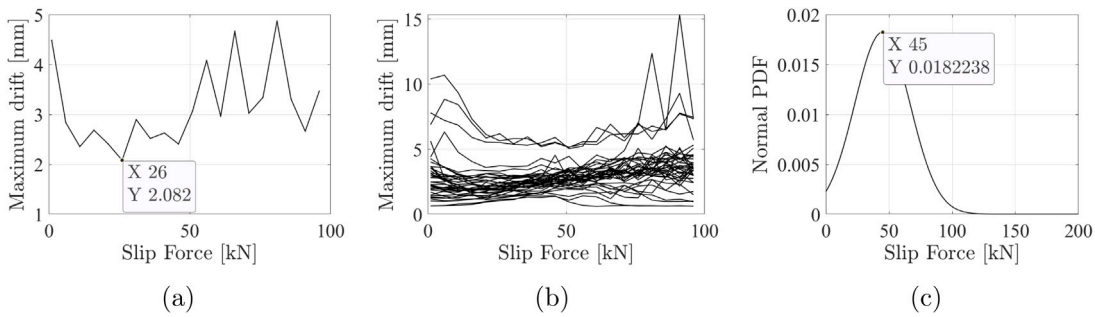

Fig. 15. (a) Maximum drift of the RC frame from the response to the El Centro earthquake as a function of the slip force; (b) Superposition of the maximum drifts of the considered system under the earthquakes in Table 4; (c) Normal distribution of the slip force values corresponding to the minimum drift.

lower displacement can generate the same dissipation. However, higher forces cause the device to activate when the RC frame has already experienced a significant displacement drift. In the considered system, characterized by strength and stiffness degradation, if the slip force is equal to 200 kN, the benefit gained from the AFC is reduced owing to its delayed intervention.

Nonetheless, the RC frame with masonry infill can exhibit a significant strength increment when compared with the same structure without infill. If R is the ratio between the slip resistance and the RC lateral capacity without the infill, the findings of this research and those reported by [29] may become more coherent. The masonry infill plays a determinant role for the correct assessment of the optimal slip force.

7. Discussion: proposal of a design procedure

The choice of the design slip force is crucial for the achievement of satisfactory seismic performance. However, the use of nonlinear dynamic analyses may be infeasible in practical applications. The exact estimation of the hysteretic response of a real structure is challenging due to the numerous uncertainties involved in modeling its inelastic response. By equaling the elastic reactions of the CLT panels with the slip resistance of n_f friction-based dampers in the same direction, the following equation holds:

$$k_{\text{clt}} \cdot d_{\text{optimum}} = n_f \cdot f_s \tag{26}$$

where k_{clt} is the lateral stiffness of the CLT panel in the ith story, f_s is the resisting slip force, d_{optimum} is the inter-story drift associated with the optimal slip force, and n_f is the number of AFCs.

In the considered case of $n_f = 1$, the percentage inter-story drift associated with the attainment of the optimal slip force is

$$d_{\text{optimum}} = \frac{f_{s,\text{optimum}}\ [\text{kN}]}{k_{\text{clt}}\ [\text{kN/mm}]} = \frac{45}{13} = 3.5\ \text{mm} \approx d_y = 3.3\ \text{mm} \tag{27}$$

where d_y is the yield of the RC frame. It is of great interest to observe that the optimal displacement demand value corresponds to the yield displacement of the RC frame. Fig. 16(a) illustrates the concept of the experimental cyclic response of the RC frame. The blue line represents the equivalent elastoplastic constitutive model of the RC frame with the masonry infill. The purple line represents the optimal drift d_{optimum}, and the red line denotes the yield displacement of the elastoplastic model of the RC frame. Fig. 16(b) shows the qualitative displacement demand–slip displacement curves. The optimal displacement corresponds to the yield displacement of the RC frame. The physical reason for the similarity between the optimal displacement and yield displacement of the RC frame is evident from Fig. 3. If $d_{\text{optimum}} \approx d_y$, the AFC possesses the highest displacement interval for energy dissipation, equal to $\delta_f = d_s - d_u$. Therefore, the preliminary design of the slip force of the AFC can be based on Eq. (27) by setting $d_{\text{optimum}} = d_y$.

The installation of the AFC and CLT panels modify the dynamic features of the structure. The CLT panels provide an incremental stiffness, which reduces the fundamental period. Therefore, the proposed

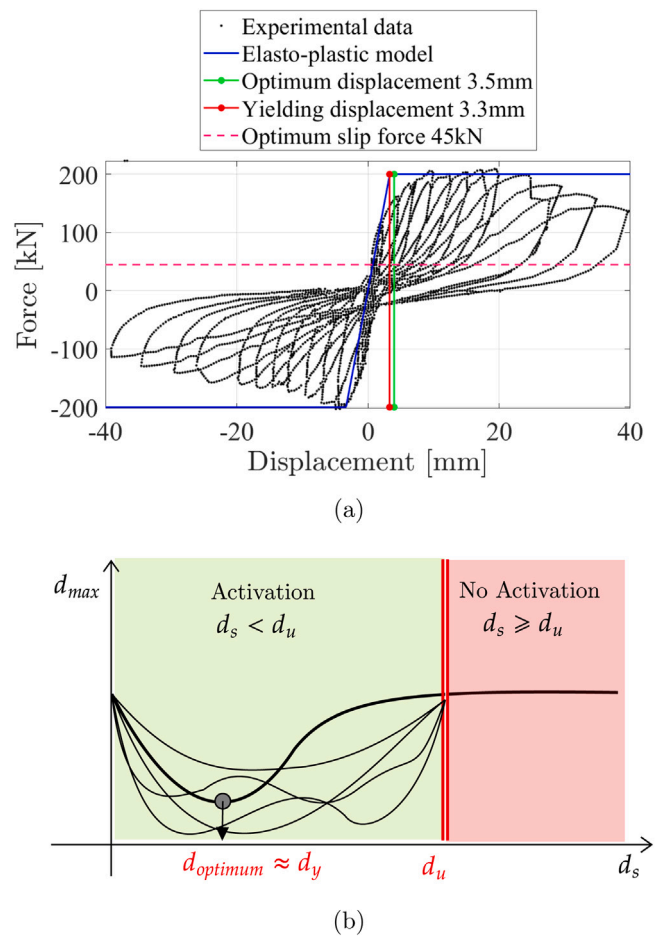

Fig. 16. (a) Representation of the inter-story drift associated with the optimal slip force, with indication of the equivalent elastoplastic behavior of the RC frame; (b) Schematic illustration of the result of the nonlinear dynamic analyses. (For interpretation of the references to colour in this figure legend, the reader is referred to the web version of this article.)

seismic retrofitting system also affects the seismic demand, causing a modification of the base shear. Thus, the designer must evaluate if the benefits from the system installation derived from the higher dissipation capacity are not canceled by a possible higher seismic demand related to the reduction in the fundamental period.

8. Conclusions

This study addressed the seismic performance of the e-CLT technology via nonlinear dynamic analysis of an elementary RC frame with

Table 4
List of earthquake recordings sorted in the descending order of PGA.

No	Year	Location (Italy)	Epicentral distance [km]	PGA [g]	Depth [km]	ML	MW
1	2016	Norcia	11.0	0.931	9.2	6.1	6.5
2	2016	Accumoli	8.5	0.851	8.1	6.0	6.0
3	2009	Fossa	3.6	0.652	17.1	5.4	5.5
4	2009	L'aquila	4.9	0.644	8.3	5.9	6.1
5	2016	Visso	7.1	0.638	7.5	5.9	5.9
6	1976	Lusevra	6.2	0.632	6.8	6.1	5.9
7	2009	Montereale	7.9	0.550	9.4	5.3	5.4
8	2012	Medolla	9.3	0.495	8.1	5.8	6.0
9	1976	Lusevra	27.7	0.346	5.7	6.4	6.4
10	1976	Gemona del friuli	16.2	0.342	11.3	6.0	6.0
11	1976	Friuli Venezia Giulia	9.4	0.322	4.3	5.8	5.6
12	1980	Laviano	33.3	0.314	15.0	6.5	6.9
13	2016	Castel Sant'Angelo sul Nera	9.4	0.295	8.1	5.4	5.4
14	2009	L'Aquila	11.0	0.294	11.0	5.1	5.4
15	2017	Cagnano amiterno	10.8	0.289	9.5	5.1	5.0
16	2009	L'Aquila	7.4	0.264	9.0	5.0	5.0
17	2012	Finale Emilia	16.1	0.259	9.5	5.9	6.1
18	2012	San Possidonio	6.9	0.252	7.2	5.1	5.5
19	1976	Nimis	7.0	0.241	13.3	5.5	5.1
20	1977	Trasaghis	7.1	0.238	10.8	5.3	5.3
21	2013	Fivizzano	11.9	0.227	7.0	5.2	5.1
22	2012	San Felice sul Panaro	7.4	0.205	5.0	5.1	9.1
23	1984	Perugia	20.6	0.201	6.0	5.2	5.6
24	2016	Norcia	4.4	0.191	8.0	5.4	5.3
25	1997	Foligno	20.1	0.184	5.5	5.4	5.4
26	1997	Foligno	21.6	0.184	5.7	5.8	6.0
27	2001	Naturno	25.9	0.167		5.3	4.8
28	1984	Villetta Barrea	17.4	0.158	12.1	5.7	5.5
29	1997	Foligno	24.2	0.152	5.7	5.6	5.7
30	2009	Pizzoli	10.1	0.148	9.7	5.0	5.1
31	1984	Settefrati	10.1	0.110	20.5	5.9	5.9
32	2012	Berceto	67.4	0.098	72.4	5.2	5.0
33	1990	Potenza	29.0	0.096	10.0	5.2	5.8
34	1997	Sellano	4.1	0.082	4.8	5.1	5.2
35	1978	Bruzzano Zeffirio	9.2	0.076	5.0	5.3	5.2
36	2004	Vobarno	13.6	0.072	5.4	5.2	5.0
37	2012	Mirabello	20.4	0.070	3.4	5.1	5.2
38	2002	Bonefro	38.1	0.057	13.0	5.4	5.7
39	2018	Molise	22.3	0.045	19.6	5.2	5.1
40	2002	Casacalenda	46.1	0.032	10.0	5.3	5.7
41	2008	Neviano degli Arduini	47.6	0.022	22.9	5.2	5.5

masonry infill. The e-CLT technology is a seismic retrofitting solution of an existing RC building based on the use of CLT panels and AFC. In an RC frame, one end of the CLT panel is fixed to the lower beam, whereas the other end is equipped with an AFC, connected to the upper beam of the RC frame. The reaching of the slip force in the AFC activates the energy dissipating device, which possibly contributes to the seismic energy absorption and reduction of the displacement drift demand. In the first part, the authors investigated the cyclic behavior of the AFC and proposed a Coulomb-like model with a friction coefficient dependent on the dissipated hysteretic energy. The experimental data were used to simulate the coupled response of a frame with masonry infill equipped with the AFC. The Atan model, which is an empirical hysteresis model proposed by [41], simulates the experimental cyclic response of an RC frame with masonry infill, as tested by [31]. The authors tested the response of the frame, represented by an SDOF oscillator with a lumped mass on the top, by using a set of 41 earthquakes and varying the slip force within a given range. Interestingly, a range of minima exists, where the slip force is associated with a significant reduction in the story drift. The displacement reduction can be higher than 50%. However, as observed by [15], the nature of seismic input significantly affects the value of the optimal slip force, which exhibits a significant scatter. The mean value of the optimal slip forces found in the considered structure was 45 kN, which was approximately 23% of the shear resistance of the frame. This evidence does not match the findings reported by [29], who predicted higher values of the optimal slip force in bare RC structural archetypes with friction dampers. In the analyses presented in this paper, the RC frame was modeled with its real behavior, including the masonry infill. The masonry infill can add a significant increment in strength and stiffness to the same RC frame without infill, in which case the results of this study would be closer to those by [29]. The authors discussed a possible design strategy based on the obtained results. The optimal displacement demand value, associated with the optimal slip force, corresponds to the yield displacement of the RC frame. This result allowed to propose a simplified design rule, which helps the practitioners to design the retrofitting intervention without having to resort to complex nonlinear analyses. Therefore, the preliminary design of the slip force of the AFC can be based on the following equation: $f_s = (k_{\mathrm{clt}} \times d_y)/n_f$, where f_s is the slip force, n_f is the number of AFCs, k_{clt} is the lateral stiffness of the CLT panel, and d_y is the yielding displacement of the RC frame. Future research efforts will focus on estimating the optimal slip force for greater number of stories.

CRediT authorship contribution statement

Angelo Aloisio: Conceptualization, Data curation, Formal analysis, Investigation, Validation, Visualization, Methodology, Resources, Software, Writing – original draft, Writing – review & editing. **Francesco Boggian:** Conceptualization, Data curation, Formal analysis, Investigation, Validation, Visualization, Methodology, Resources, Software, Writing – original draft, Writing – review & editing. **Roberto Tomasi:** Funding acquisition, Supervision, Project administration, Validation, Resources, Writing – review & editing.

Declaration of competing interest

The authors declare that they have no known competing financial interests or personal relationships that could have appeared to influence the work reported in this paper.

Data availability statement

Some or all data, models, or code that support the findings of this study are available from the corresponding author upon reasonable request.

Funding

This study was conducted in the framework of the "Energy and seismic affordable renovation solutions" (e-SAFE) project, which has received funding from the European Union's Horizon 2020 Research and Innovation Programme under grant agreement No. 893135. Neither the Executive Agency for Small and Medium-sized Enterprises (EASME) nor the European Commission is in any way responsible for any use that may be made of the information contained in this paper.

References

[1] Milman MH, Chu C-C. Optimization methods for passive damper placement and tuning. J Guid Control Dyn 1994;17(4):848–56.
[2] Levy R, Lavan O. Fully stressed design of passive controllers in framed structures for seismic loadings. Struct Multidiscip Optim 2006;32(6):485–98.
[3] Takewaki I. Building control with passive dampers: optimal performance-based design for earthquakes. John Wiley & Sons; 2009.
[4] Pall AS, Marsh C, et al. Response of friction damped braced frames. J Struct Eng 1982;108(9):1313–23.
[5] Nakashima M, Saburi K, Tsuji B. Energy input and dissipation behaviour of structures with hysteretic dampers. Earthq Eng Struct Dyn 1996;25(5):483–96.
[6] Tsampras G, Sause R, Zhang D, Fleischman RB, Restrepo JI, Mar D, et al. Development of deformable connection for earthquake-resistant buildings to reduce floor accelerations and force responses. Earthq Eng Struct Dyn 2016;45(9):1473–94.
[7] Tsampras G, Sause R, Fleischman RB, Restrepo JI. Experimental study of deformable connection consisting of friction device and rubber bearings to connect floor system to lateral force resisting system. Earthq Eng Struct Dyn 2018;47(4):1032–53.
[8] Eldin MN, Dereje AJ, Kim J. Seismic retrofit of RC buildings using self-centering PC frames with friction-dampers. Eng Struct 2020;208:109925.
[9] Javidan MM, Kim J. Seismic retrofit of soft-first-story structures using rotational friction dampers. J Struct Eng 2019;145(12):04019162.
[10] Cho C-G, Kwon M. Development and modeling of a frictional wall damper and its applications in reinforced concrete frame structures. Earthq Eng Struct Dyn 2004;33(7):821–38.
[11] Fitzgerald T, Anagnos T, Goodson M, Zsutty T. Slotted bolted connections in aseismic design for concentrically braced connections. Earthq Spectra 1989;5(2):383–91.
[12] Popov EP, Grigorian CE, Yang T-S. Developments in seismic structural analysis and design. Eng Struct 1995;17(3):187–97.
[13] Grigorian CE, Yang T-S, Popov EP. Slotted bolted connection energy dissipators. Earthq Spectra 1993;9(3):491–504.
[14] Clifton G, MacRae G, Mackinven H, Pampanin S, Butterworth J. Sliding hinge joints and subassemblies for steel moment frames. In: Proc Of New Zealand Society for earthq eng conf. Palmerston North, New Zealand: 2007.
[15] Filiatrault A, Cherry S. Seismic design spectra for friction-damped structures. J Struct Eng 1990;116(5):1334–55.
[16] Loo WY, Kun C, Quenneville P, Chouw N. Experimental testing of a rocking timber shear wall with slip-friction connectors. Earthq Eng Struct Dyn 2014;43(11):1621–39.
[17] Hashemi A, Zarnani P, Masoudnia R, Quenneville P. Experimental testing of rocking cross-laminated timber walls with resilient slip friction joints. J Struct Eng 2018;144(1):04017180.
[18] Hashemi A, Bagheri H, Yousef-Beik SMM, Darani FM, Valadbeigi A, Zarnani P, et al. Enhanced seismic performance of timber structures using resilient connections: Full-scale testing and design procedure. J Struct Eng 2020;146(9):04020180.
[19] Margani G, Evola G, Tardo C, Marino EM. Energy, seismic, and architectural renovation of RC framed buildings with prefabricated timber panels. Sustainability 2020;12(12):4845.
[20] Mackinven H. Sliding Hinge Joint for steel moment frames experimental testing. Unpublished ENCI493 Project Report, Department Of Civil Engineering; 2006.
[21] Khoo H-H, Clifton C, Butterworth J, MacRae G, Ferguson G. Influence of steel shim hardness on the sliding hinge joint performance. J Constr Steel Res 2012;72:119–29.
[22] Aloisio A, Alaggio R, Fragiacomo M. Fragility functions and behavior factors estimation of multi-story cross-laminated timber structures characterized by an energy-dependent hysteretic model. Earthquake Spectra 2021;37(1):134–59. http://dx.doi.org/10.1177/8755293020936696.
[23] Aloisio A, Boggian F, Tomasi R, Fragiacomo M. Reliability-based assessment of LTF and CLT shear walls under in-plane seismic loading using a modified bouc-wen hysteresis model. ASCE-ASME J Risk Uncertainty Engrg Syst, Part A: Civil Engrg 2021;7(4):04021065. http://dx.doi.org/10.1061/AJRUA6.0001161.
[24] Aloisio A, Alaggio R, Fragiacomo M. Equivalent viscous damping of cross-laminated timber structural archetypes. J Struct Engrg 2021;147(4):04021012. http://dx.doi.org/10.1061/%28ASCE%29ST.1943-541X.0002947.
[25] Tardo C, Boggian F, Hatletveit M, Marino E, Margani G, Tomasi R. Mechanical characterization of energy dissipation devices in retrofit solution of reinforced concrete frames coupled with solid wood panels. In: Proc Of The 12th International Conference On Structural Analysis Of Historical Constructions. Barcelona, Spain: 2021.
[26] Moreschi L, Singh M. Design of yielding metallic and friction dampers for optimal seismic performance. Earthq Eng Struct Dyn 2003;32(8):1291–311.
[27] Nabid N, Hajirasouliha I, Petkovski M. Performance-based optimisation of RC frames with friction wall dampers using a low-cost optimisation method. Bull Earthq Eng 2018;16(10):5017–40.
[28] Miguel LFF, Miguel LFF, Lopez RH. Simultaneous optimization of force and placement of friction dampers under seismic loading. Eng Optim 2016;48(4):582–602.
[29] Nabid N, Hajirasouliha I, Petkovski M. A practical method for optimum seismic design of friction wall dampers. Earthq Spectra 2017;33(3):1033–52.
[30] Golondrino JC, MacRae G, Clifton C. Behaviour of asymmetrical friction connections using different shim materials. In: Proc of the New Zealand Society for earthquake engineering conference. Christchurch, New Zaeland: 2012.
[31] Cavaleri L, Di Trapani F. Cyclic response of masonry infilled RC frames: Experimental results and simplified modeling. Soil Dyn Earthq Eng 2014;65:224–42.
[32] Sirotti S, Pelliciari M, Di Trapani F, Briseghella B, Marano GC, Nuti C, Tarantino AM. Development and validation of new bouc–wen data-driven hysteresis model for masonry infilled rc frames. J Engrg Mech 2021;147(11):04021092.
[33] Hajirasouliha I, Asadi P, Pilakoutas K. An efficient performance-based seismic design method for reinforced concrete frames. Earthq Eng Struct Dyn 2012;41(4):663–79.
[34] Fitzgerald D, Miller TH, Sinha A, Nairn JA. Cross-laminated timber rocking walls with slip-friction connections. Eng Struct 2020;220:110973.
[35] EN14399-4. High-strength structural bolting assemblies for preloading. System HV. Hexagon bolt and nut assemblies. CEN - European Committee For Standardization; 2015.
[36] EN1090-2. Execution of steel structures and aluminium structures - Part 2: Technical requirements for steel structures. CEN - European Committee For Standardization; 2018.
[37] Boggian F, Tardo C, Aloisio A, Marino E, Tomasi R. Experimental cyclic response of a novel friction connection for seismic retrofitting of rc buildings with clt panels. J Struct Eng 2022. http://dx.doi.org/10.1061/(ASCE)ST.1943-541X.0003313.
[38] Marthinsen Birch Aune, M. Experimental assessment of a steel dissipating system. Norwegian University of Life Sciences; 2020.
[39] ISO16670. Timber structures — Joints made with mechanical fasteners — Quasi-static reversed-cyclic test method. ISO - International Organization for Standardization); 2003.
[40] EN15129. Anti-seismic devices. CEN - European Committee For Standardization; 2018.
[41] Aloisio A, Sejkot P, Iqbal A, Fragiacomo M. An empirical transcendental hysteresis model for structural systems with pinching and degradation. Earthq Eng Struct Dyn 2021;50(9):2277–93. http://dx.doi.org/10.1002/eqe.3442.
[42] Foliente GC. Hysteresis modeling of wood joints and structural systems. J Struct Eng 1995;121(6):1013–22.
[43] Aloisio A, Alaggio R, Köhler J, Fragiacomo M. Extension of generalized Bouc-Wen hysteresis modeling of wood joints and structural systems. J Eng Mech 2020;146(3):04020001. http://dx.doi.org/10.1061/(ASCE)EM.1943-7889.0001722.
[44] Aloisio A, Boggian F, Tomasi R, Fragiacomo M. The role of the hold-down in the capacity model of LTF and CLT shear walls based on the experimental lateral response. Constr Build Mater 2021;289:123046. http://dx.doi.org/10.1016/j.conbuildmat.2021.123046.
[45] EN12512. Timber structures. Test methods. Cyclic testing of joints made with mechanical fasteners. CEN - European Committee For Standardization; 2022.
[46] Brandner R, Flatscher G, Ringhofer A, Schickhofer G, Thiel A. Cross laminated timber (CLT): Overview and development. Eur J Wood Wood Products 2016;74(3):331–51.

[47] Ministero delle Infrastrutture e dei Trasporti. NTC2008–Norme tecniche per le costruzioni. tech. rep., DM 14/01/2008, 2008, [in Italian].
[48] Ferreira F, Moutinho C, Cunha A, Caetano E. An artificial accelerogram generator code written in Matlab. Eng Rep 2020;2(3):e12129.
[49] Petkovski M, Waldron P. Optimum friction forces for passive control of the seismic response of multi-storey buildings. In: Proc of the 40 years of European earthquake engineering. 2003.
[50] Fallah N, Honarparast S. NSGA-II based multi-objective optimization in design of pall friction dampers. J Construct Steel Res 2013;89:75–85.